Electronic Supplementary Material (ESI) for Nanoscale.

Electronic Properties of Single Prussian Blue Analog Nanocrystals Determined by Conductive-AFM.

Hugo Therssen[1], Laure Catala[2], Sandra Mazérat[2], Talal Mallah[2], Dominique Vuillaume[1], Thierry Mélin[1], Stéphane Lenfant[1]

1. *Univ. Lille, CNRS, Univ. Polytechnique Hauts-de-France, UMR 8520 - IEMN - Institut d'Electronique de Microélectronique et de Nanotechnologie, F-59000 Lille, France.*
2. *Institut de Chimie Moléculaire et des Matériaux d'Orsay (ICMMO), CNRS, Université Paris-Saclay, 91400 Orsay Cedex, France.*

SUPPORTING INFORMATION

1. Synthesis of the PBA nanocrystals

15 nm nanocrystals (CsCoFe_15). An aqueous solution (100 ml) containing 69.4 mg ($4x10^{-3}$ ML^{-1}) of CsCl and 47.7 mg ($2x10^{-3}$ ML^{-1}) of $[Co(H_2O)_6]Cl_2$ is prepared. Then another aqueous solution (100 ml) containing 67.6 mg ($2x10^{-3}$ ML^{-1}) of $K_3[Fe(CN)_6]$ is prepared. The two solutions were mixed and vigorously stirred leading to the CsCoFe_15 nanocrystals.

30 nm nanocrystals (CsCoFe_30). An aqueous solution (240 ml) containing 122.2 mg ($3x10^{-3}$ ML^{-1}) of CsCl and 87.2 mg ($1.5x10^{-3}$ ML^{-1}) of $[Co(H_2O)_6]Cl_2$ is prepared. Then another aqueous solution (240 ml) containing 87.2 mg ($1.5x10^{-3}$ ML^{-1}) of $K_3[Fe(CN)_6]$ is prepared.

The two solutions were added simultaneously using a peristaltic pump (1 ml/minute) onto 50 ml of the previous solution containing the 15 nm nanocrystals, completed with 20 ml of water, that play the role of seeds for the growth of the objects leading to CsCoFe_30 nanocrystals.

50 nm nanocrystals (CsCoFe_50). An aqueous solution (180 ml) containing 92.4 mg ($3x10^{-3}$ ML^{-1}) of CsCl and 65.4 mg ($1.5x10^{-3}$ ML^{-1}) of $[Co(H_2O)_6]Cl_2$ is prepared. Then another aqueous solution (240 ml) containing 89.4 mg ($1.5x10^{-3}$ ML^{-1}) of $K_3[Fe(CN)_6]$ is prepared.

The two solutions were added simultaneously using a peristaltic pump (1 ml/minute) onto 100 ml of the previous solution containing the 30 nm nanocrystals, completed with 40 ml of water, that play the role of seeds for the growth of the 50 nm objects leading to CsCoFe_50 nanocrystals.

The size of the objects corresponds to hydrodynamic diameter measured by DLS as depicted in the Figure S1.

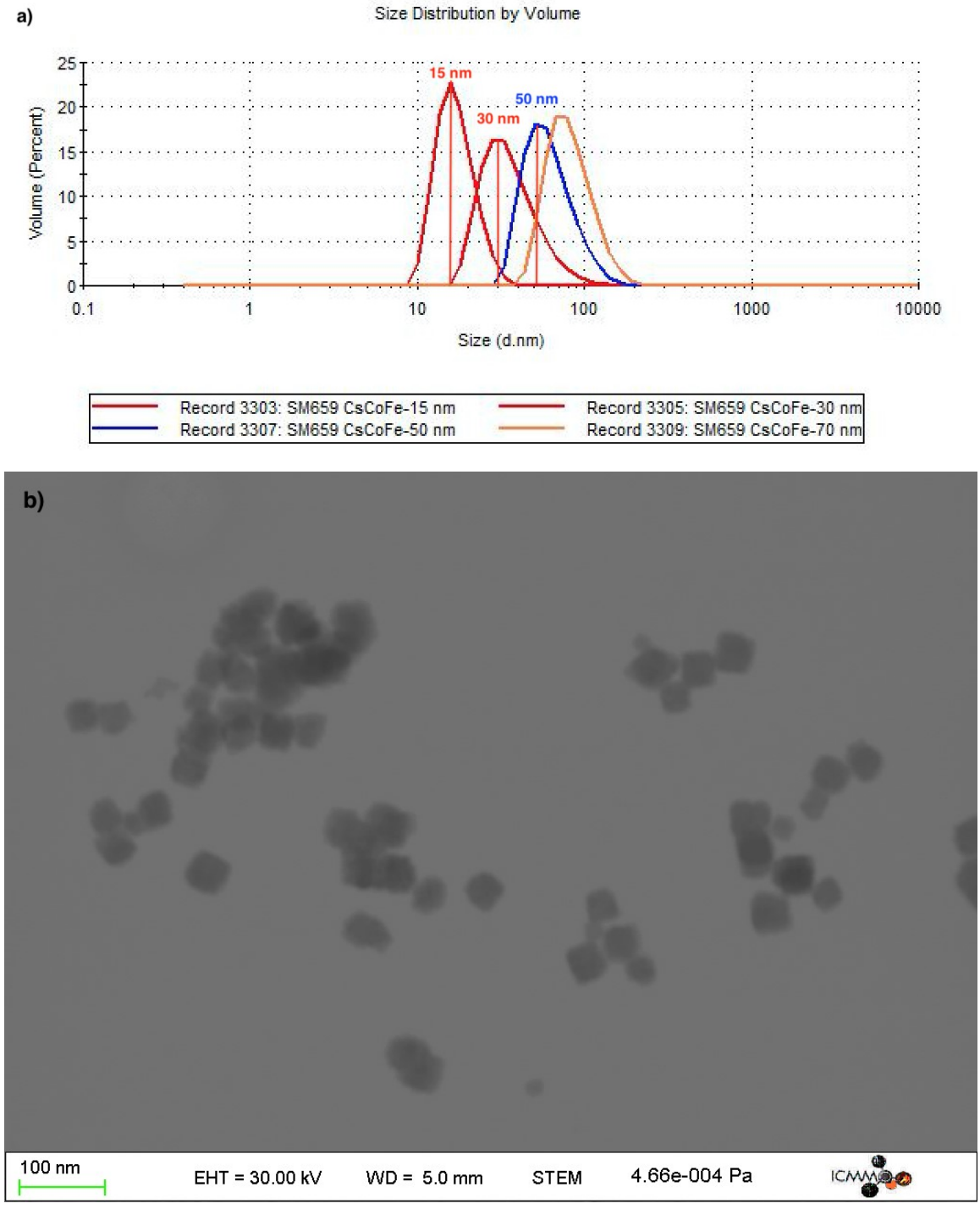

Figure S1. *a) Hydrodynamic diameter of the objects for the three synthesis steps (the plot for the higher diameter objects is shown to demonstrate that this synthesis protocol can be used to prepare objects of a size larger than 50 nm, here 70 nm), b) Transmission electron microscopy image of a sample of CsCoFe_50 showing the cubic shape of the nanocrystals as*

expected[1] *and showing a relatively large distribution of size that is very narrow for the pristine objects. The large distribution is due to the two-step preparation process that leads from the 15 to the 50 nm samples.*

2. Current-voltage 2D histogram measured on the bare HOPG substrates

It is known that bare HOPG substrates have a large dispersion of conductance (Fig. S2) depending on the exact sheets, ribbons, step edges contacted by the tip of the C-AFM with current from tens of nA (at low voltage <1V) up to µA and larger.[2]

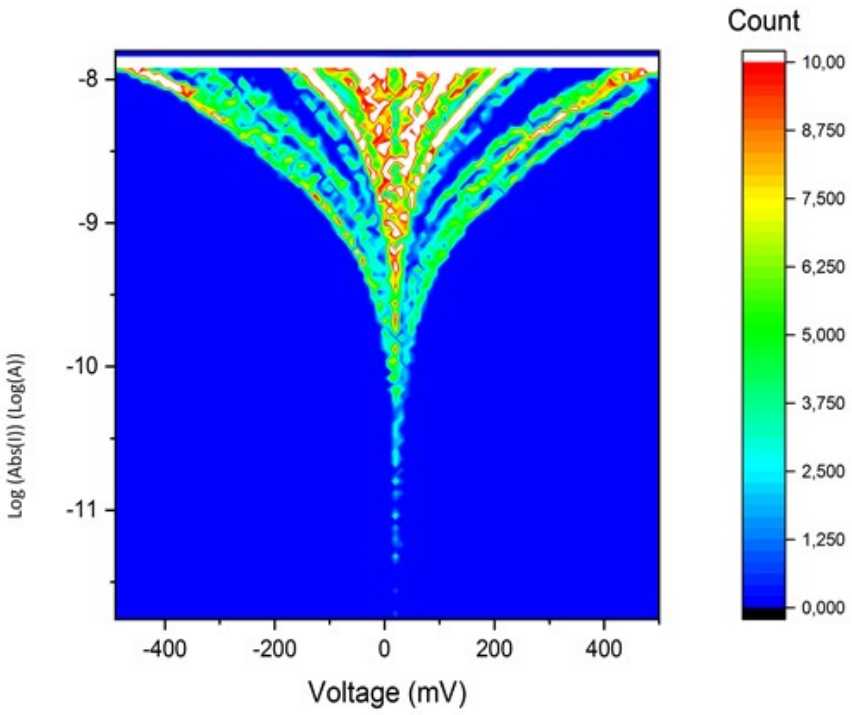

Figure S2. *2D histogram of the HOPG substrate used for the NC deposition with a mean current measured by C-AFM; log-$\bar{I}$ superior to -8.5 (corresponding to $\bar{I} > 3 \times 10^{-9}$ A) at 0.4 V.*

3. Supplementary I(V) datasets and analysis

On every samples, 2 to 3 NCs were measured following the same protocol as for the dataset shown and discussed in the main text (Figs.4, 6, 7).

Dataset #2

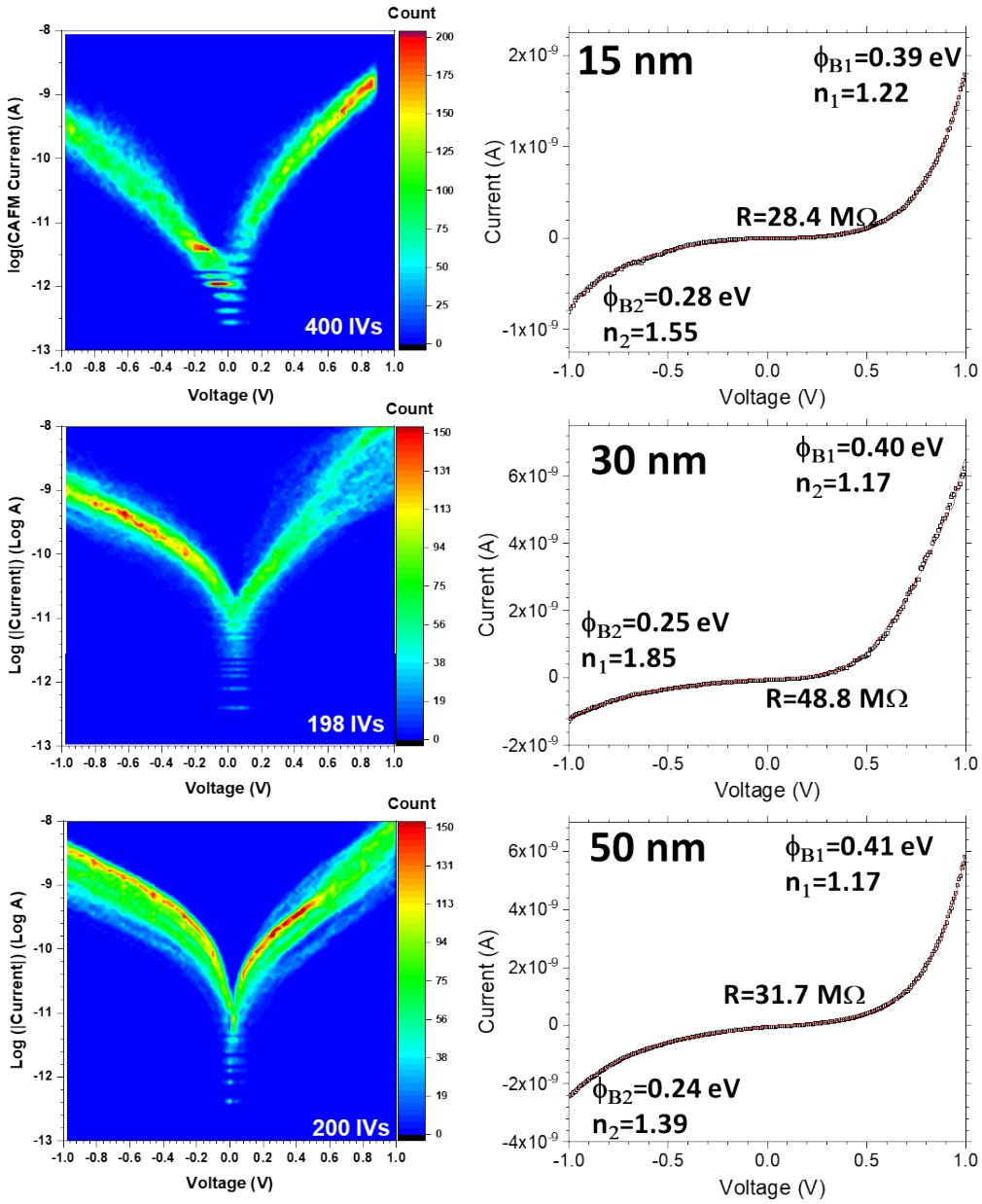

Dataset #3

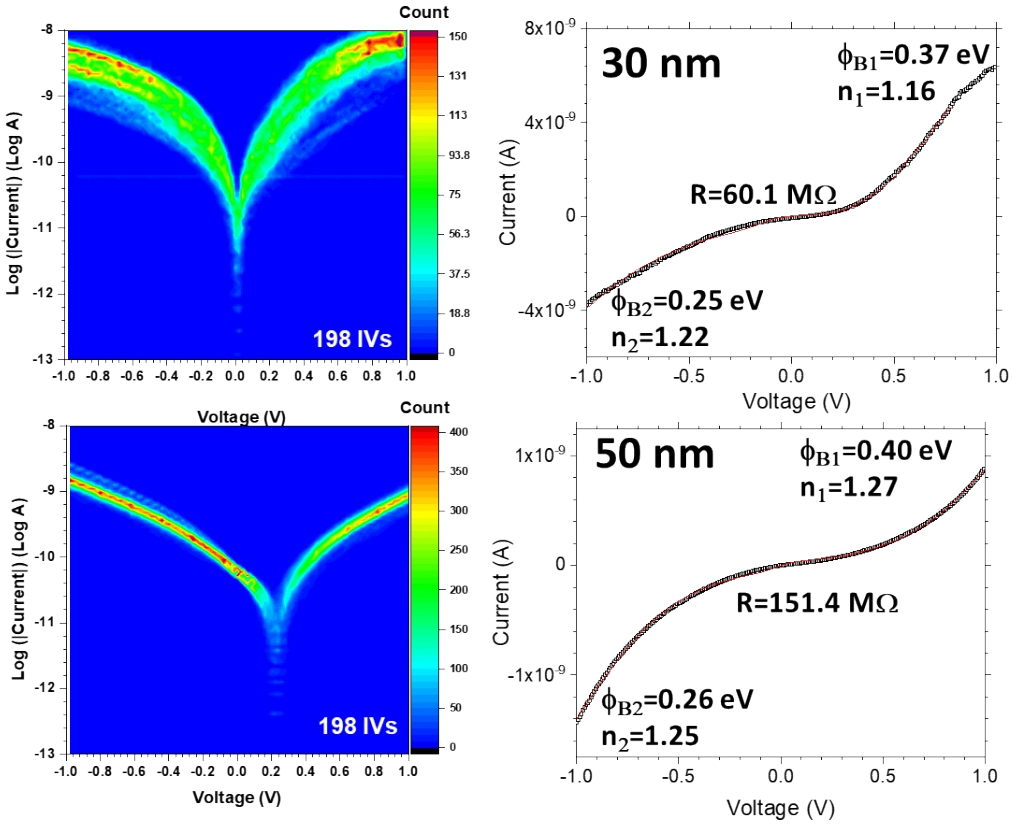

Figure S3. *C-AFM 2D current-voltage I(V) histograms obtained with around 200 IVs traces for PBA NCs (Dataset #2 and #3) (Left), and the corresponding mean $\bar{I}$(V) curves (black line) (Right) adjusted using the double SB model and by adjusting parameters: the effective SBs ($\Phi_{B1,B2}$), the ideality factors ($n_{1,2}$) and the intrinsic resistance R (red lines).*

4. Estimation of the contact area at the NC/C-AFM interface using a Hertzian model

We estimate the electrical contact surface for a loading force of 15 nN using a Hertzian model:[3]

$$S_2 = \pi\left(\frac{3R\,F_{applied}}{4E^*}\right)^{\frac{2}{3}} \quad \text{(S1)}$$

where R is the radius of the C-AFM tip (fixed at 25 nm according to the manufacturer), $F_{applied}$ the tip load force (15nN), E^* the reduced effective Young modulus defined as:

$$E^* = \left(\frac{1-\gamma_{NC}^2}{E_{NC}} + \frac{1-\gamma_{tip}^2}{E_{tip}}\right)^{-1} \quad \text{(S2)}$$

with $E_{NC/tip}$ and $\gamma_{NC/tip}$ the Young modulus and the Poisson ratio of the NC and the C-AFM tip respectively. The Young modulus of CsCoFe NCs is not known. A value of 43 GPa was reported for bulk material.[4] Values of about 30 GPa and 24 GPa were measured for 3 nm and 115 nm NCs of another material (Ni/[Fe(CN)$_6$]).[5]

By using the following values E_{tip} = 204 GPa,[6] E_{NC} = 24 GPa (by default, see above), [5] γ_{tip} = 0.37[6] and γ_{NC} = 0.36,[5] we estimate a surface S_2 ~ 16 nm². This Hertzian model gives an estimation of the NC elastic deformation close here to 0.2 nm, negligible compared to the size of the NC.

5. Statistical analysis of the dataset in Fig. 3 and in Fig. S3

The DSB model was fitted on all the individuals I(V) curves of the dataset to construct the statistical distribution of the model parameters shown in Fig. 3, main text (Dataset #1) and in Fig S3 (Dataset #2 and #3).

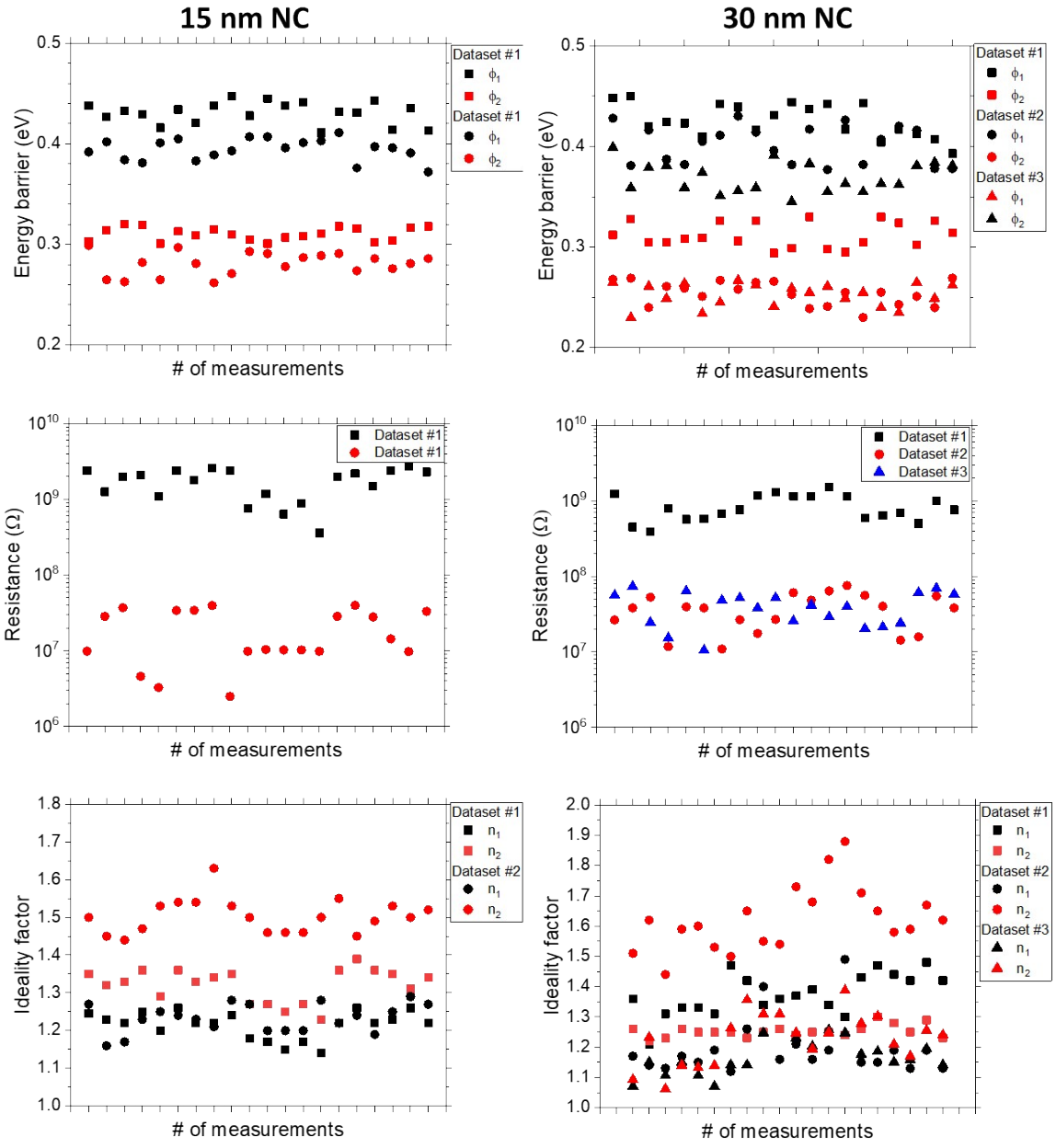

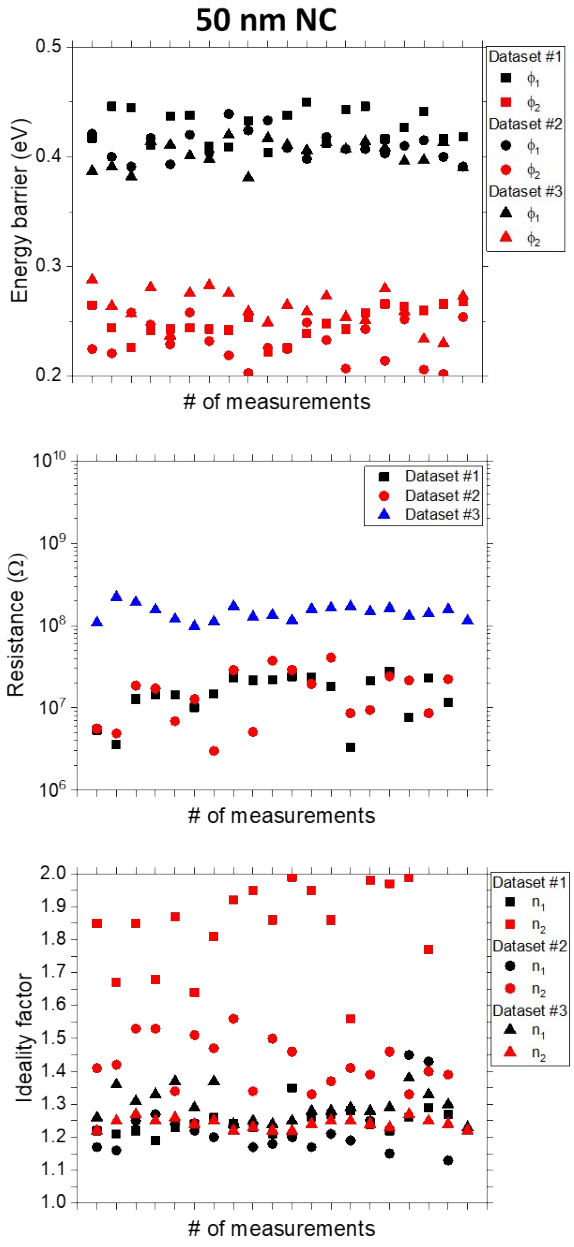

Figure S4*. Statistical distributions of the fitted model values obtained with the fitting with the double SB model and by adjusting parameters: the effective SBs (*$\Phi_{B1,B2}$*), the ideality factors (*$n_{1,2}$*) and the intrinsic resistance R, on a random sample of 20 I(V)s curves extract in the complete datasets presented in Fig. 3 and Fig. S3 to obtain an estimation of the statistical distribution of the parameters.*

6. Ideality factors.

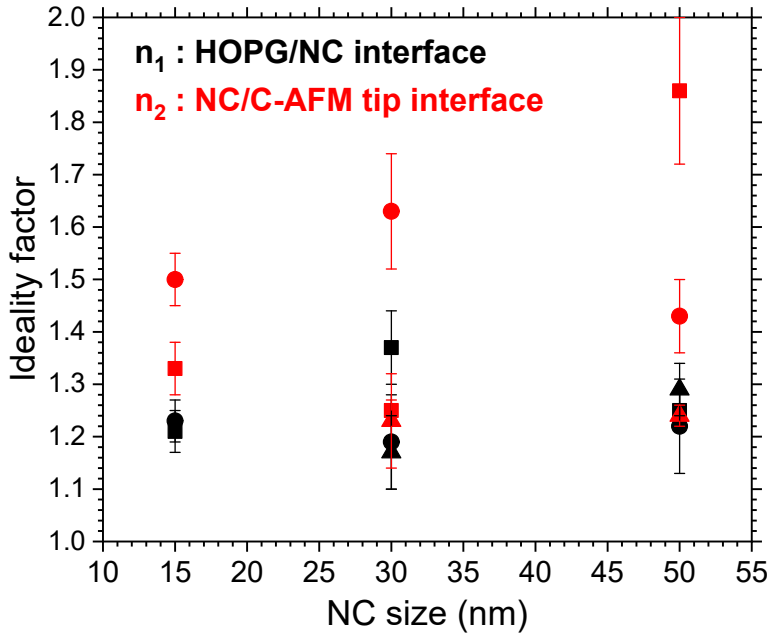

Figure S5. *Evolution of the ideality factor of the two CsCoFe NC Schottky diodes. The values refer to the dataset #1 shown in Fig. 3 (square symbols), dataset #2 in Fig. S3 (circle symbols), and dataset #3 in Fig. S3 (triangle symbols).*

7. Estimation of the NC conductivity.

The basic equation to estimate the conductivity σ from the resistance R is : $G=(R)^{-1}=\sigma\ S/L$ for a regular tube of surface S and length L, of equivalently $G=(R)^{-1}=\sigma\ V/L^2$ with V the volume of the material contacted between the two electrodes. Here, we consider a truncate pyramidal device with asymmetric contacts at the HOPG/NC and at the NC/PtIr tip (see scheme in Figure S6). For a truncated pyramid inside the nanocube of side a, the volume is given by $V = a(a^2+ar+r^2)/3$, thus we used $G=\sigma(a+r+r^2/a)/3$ to estimate the conductivity, with a the NC size, r = 4 nm.

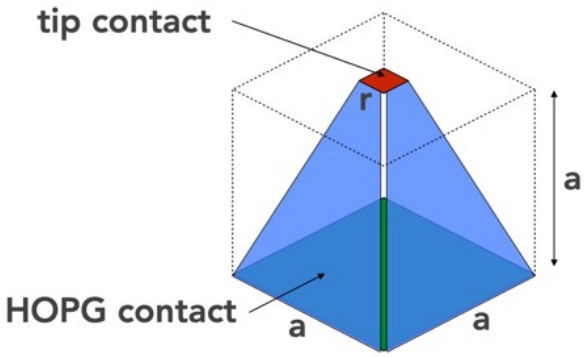

Figure S6. *Truncate pyramidal device with asymmetric contacts at the HOPG/NC and at the NC/PtIr tip considered for the estimation of the NC conductivity.*

8. I(V) analysis using the single-energy level (SEL) model

The single-energy level (SEL) model (Eq. 3), considers that: i) a single molecular orbital (MO) dominates the charge transport, ii) the voltage mainly drops at the molecule/electrode interface and iii) that the MO broadening is described by a Lorentzian or Breit-Wigner distribution.[7,8] The simple energy scheme (inset Fig. S7) is described by ε_0 the energy of the MO involved in the transport (with respect to the Fermi energy of the electrodes), Γ_1 and Γ_2 the electronic coupling energy between the MO and the electron clouds in the two electrodes, e the elementary electron charge, h the Planck constant. This analytical model reads:

[redacted] (S3)

This model is valid at 0 K, since the Fermi-Dirac electron distribution of the electrodes is not taken into account. However, it was shown that it can be reasonably used to fit data measured at room temperature for voltages below the transition between the off-resonant and resonant transport conditions at which the broadening of the Fermi function modify the I-V shape leading to sharpened increase of the current.[9-11] Moreover, for the sake of comparison with the I(V)s previously measured for multi-NCs devices, which were acquired

between -0.5 and 0.5 V,[12] we limited the fit of Eq. S3 to this voltage window. We verified that the condition of applicability of the 0K SEL model to room temperature experimental data is satisfied (here with $\varepsilon_0 < 0.5$ eV, Γ_1 and Γ_2 around 0.1-1 meV, this condition is $|V|<0.64$ V).[13] The fits were done with the routine included in ORIGIN software (version 2019, OriginLab Corporation, Northampton, MA, USA), using the method of least squares and the Levenberg Marquardt iteration algorithm. Figure S7 shows the fits on the average I(V) of the three datasets shown Fig. 3 and Fig. S3. The fitted energy ε_0 and the electrode coupling energies Γ_1 and Γ_2 are summarized in Figs.S8 and S9, respectively.

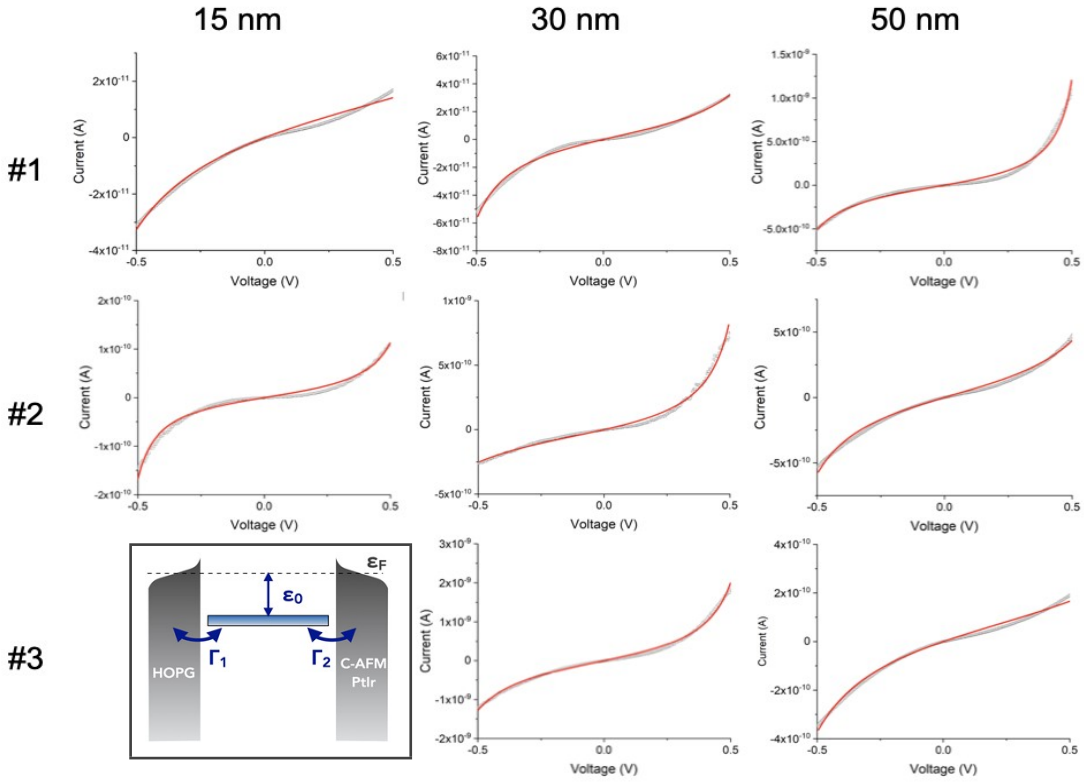

Figure S7*. Fits of the SEL model (red lines) on the average I(V) (open squares) for the three datasets (no data at 15 nm for the dataset #3). The inset shows the energy scheme of the HOPG/NC/PtIr device with the SEL model parameters.*

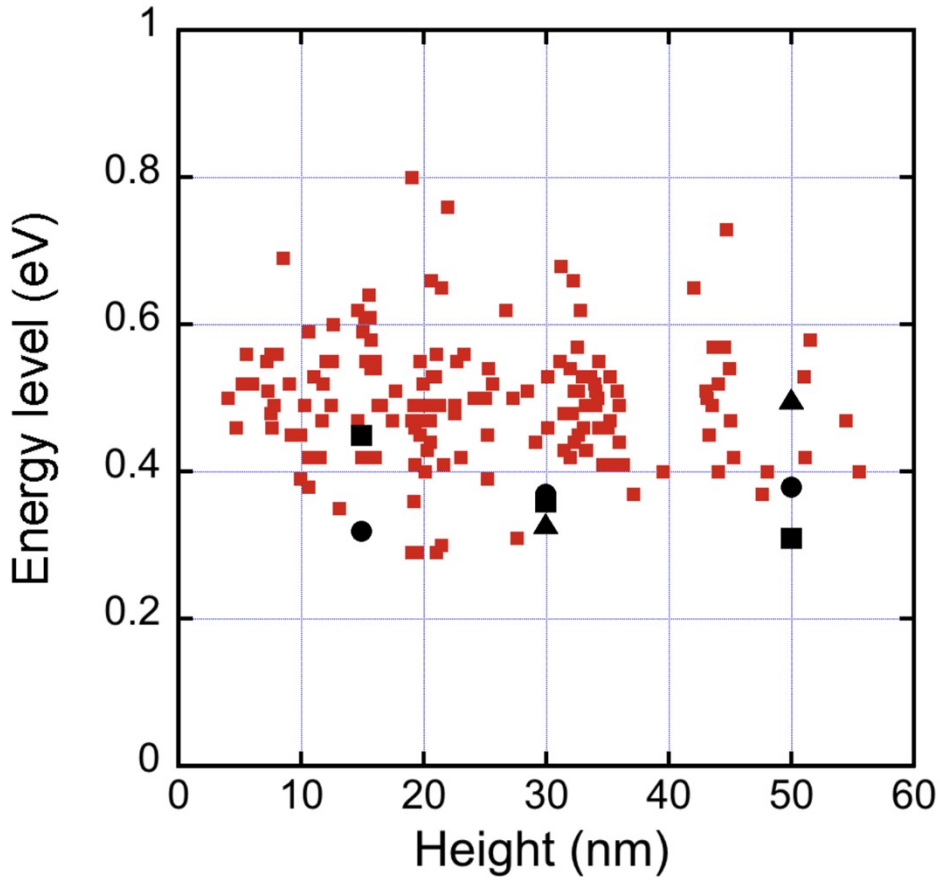

Figure S8. *Energy levels ε_0 obtained from the SEL model (fits shown in Fig. S7): dark squares (dataset #1), dark circles (dataset #2), dark triangles (dataset #3). The red symbols are the full statistics for the multi-NCs devices (from Fig. S18 in the ESI of Ref. [12]).*

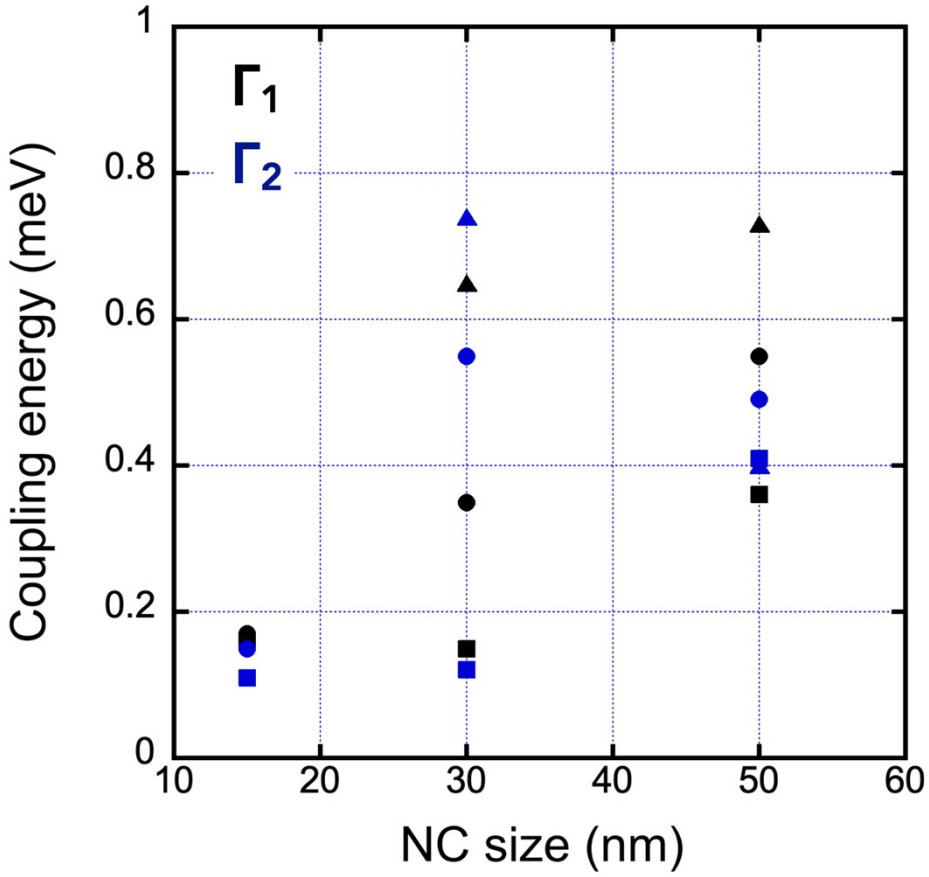

Figure S9*. Evolution of the electrode coupling energies Γ_1 and Γ_2 versus the NC size: square symbols (dataset #1), circle symbols (dataset #2), triangle symbols (dataset #3).*

References

1. L. Trinh, S. Zerdane, S. Mazerat, N. Dia, D. Dragoe, C. Herrero, E. Riviere, L. Catala, M. Cammarata, E. Collet and T. Mallah, *Inorg. Chem.*, 2020, **59**, 13153-13161.
2. S. Banerjee, M. Sardar, N. Gayathri, A. K. Tyagi and B. Raj, *Physical Review B*, 2005, **72**.
3. D. J. Wold and C. D. Frisbie, *J. Am. Chem. Soc.*, 2001, **123**, 5549-5556.
4. A. Bleuzen, J. D. Cafun, A. Bachschmidt, M. Verdaguer, P. Munsch, F. Baudelet and J. P. Itie, *Journal of Physical Chemistry C*, 2008, **112**, 17709-17715.
5. G. Felix, M. Mikolasek, H. J. Shepherd, J. Long, J. Larionova, Y. Guari, J. P. Itie, A. I. Chumakov, W. Nicolazzi, G. Molnar and A. Bousseksou, *European Journal of Inorganic Chemistry*, 2018, 443-448.
6. V. Prudkovskiy, I. Arbouch, A. Leaustic, P. Yu, C. Van Dyck, D. Guerin, S. Lenfant, T. Mallah, J. Cornil and D. Vuillaume, *Nanoscale*, 2022, **14**, 5725-5742.
7. S. Datta, *Electronic transport in mesoscopic systems*, Cambridge university press, 1997.
8. J. C. Cuevas and E. Scheer, *Molecular Electronics: An introduction to theory and experiment*, World Scientific, 2010.
9. L. Grüter, F. Cheng, T. T. Heikkilä, M. T. González, F. Diederich, C. Schönenberger and M. Calame, *Nanotechnology*, 2005, **16**, 2143-2148.
10. J. P. Bourgoin, D. Vuillaume, M. Goffman and A. Filoramo, in *Nanoscience*, eds. C. Dupas, P. Houdy and M. Lahmani, Springer, Berlin, 2007.
11. J. Brunner, Basel University, 2013.
12. R. Bonnet, S. Lenfant, S. Mazerat, T. Mallah and D. Vuillaume, *Nanoscale*, 2020, **12**, 20374-20385.
13. I. Baldea, *Phys. Chem. Chem. Phys.*, 2023, **25**, 19750-19763.